

Strong Algorithmic Cooling in Large Star-Topology Quantum Registers

†Varad R. Pande, †Gaurav Bhole, †Deepak Khurana, and †,‡T. S. Mahesh*

†*Department of Physics and NMR Research center,*

‡*Center for Energy Sciences,*

Indian Institute of Science Education and Research, Pune

Cooling the qubit into a pure initial state is crucial for realizing fault-tolerant quantum information processing. Here we envisage a star-topology arrangement of reset and computation qubits for this purpose. The reset qubits cool or purify the computation qubit by transferring its entropy to a heat-bath with the help of a heat-bath algorithmic cooling procedure. By combining standard NMR methods with powerful quantum control techniques, we cool central qubits of two large star-topology systems, with 13 and 37 spins respectively. We obtain polarization enhancements by a factor of over 24, and an associated reduction in the spin temperature from 298 K down to 12 K. Exploiting the enhanced polarization of computation qubit, we prepare combination-coherences of orders up to 15. By benchmarking the decay of these coherences we investigate the underlying noise process. Further, we also cool a pair of computation qubits and subsequently prepare them in an effective pure-state.

I. INTRODUCTION

Quantum information processors and other quantum devices are expected to have a major impact on future technologies. Initializing qubits - the building blocks of a quantum memory, into a deterministic initial state is an essential process that precedes other quantum operations [1, 2]. This process is important not only for quantum registers with low-purity initial states, but also for achieving scalable quantum processors with the help of quantum error correction [3]. While there are many ways to enhance the purity of a spin-qubit, from optical pumping (eg. [4]) to exploiting para-hydrogens (eg. [5]), polarization-transfer remains the simplest approach. Transferring polarization from one spin to another has long been a routine operation in NMR spectroscopy [6]. Inspired by the spin dynamics in these NMR experiments, a universal bound for such entropy transfers in closed systems was calculated by Sørensen [7]. Later Shulman and Vazirani designed an algorithmic approach for transferring entropy from a smaller set of *computation* qubits, to a larger set of so called *reset* qubits [8]. This method, generally known as algorithmic cooling (AC), is essentially a unitary process. A non-unitary extension of the above pairwise entropy compression between successive qubits was proposed by Boykin *et al.* [9] which resulted in the heat-bath algorithmic cooling (HBAC). Here, the reset qubits periodically release their excess entropy to a heat-bath so that higher cooling of the computation qubit can be achieved by constructive iterations of AC. Since then, several HBAC algorithms have been proposed [10–14] and numerous experimental studies have also been reported [15–21] which use three or five qubit entropy compression circuits as the building block for AC. More recently asymptotic bounds for HBAC algorithms have been estimated numerically by Raeisi *et*

al. [22] as well as analytically by Rodríguez-Briones *et al.* [23]. Here we consider HBAC in star-topology quantum registers, which offer highly efficient platforms for this purpose, allowing entropy compression between the computation qubit and a large number of reset qubits.

In the following section, we first describe star-topology systems and then explain HBAC procedure in such systems. Subsequently, in section III, we describe NMR experiments of HBAC on two star-topology quantum registers consisting of 13 and 37 spins respectively. As an application of HBAC, we report the preparation of large combination coherences in section III B. We have also reported benchmarking the decay of these coherences and attempt to understand the dominant source of noise. Before we summarize, we also explain, in section III C, the sequential HBAC of a pair of computation qubits, and subsequently preparing them into an effective pure state.

II. THEORY

A. Star-topology quantum register

In star-topology, a single *computation* qubit (**C**) is uniformly coupled to a set of N identical (magnetically equivalent) *reset* qubits (**R**) with the same interaction strength J_{RC} (Fig. 1). The interactions among the reset qubits are assumed to be either negligible or, as in our case, ineffective due to magnetic equivalence symmetry. Star-topology quantum systems have already found several interesting applications such as in field sensing [24], spectroscopic measurements [25], as well as for understanding noise in quantum systems [26].

In the NMR setting described here, the qubits are formed by spin-1/2 nuclei of a molecular ensemble placed in a strong static magnetic field $B_0\hat{z}$. For effectiveness, we choose the computation and reset qubits to be of different nuclear isotopes with Larmor frequencies $\omega_0^C = -\gamma_C B_0$ and $\omega_0^R = -\gamma_R B_0$ respectively, where γ_C, γ_R are the gyromagnetic ratios such that $\gamma = \gamma_R/\gamma_C \geq 1$.

* mahesh.ts@iiserpune.ac.in

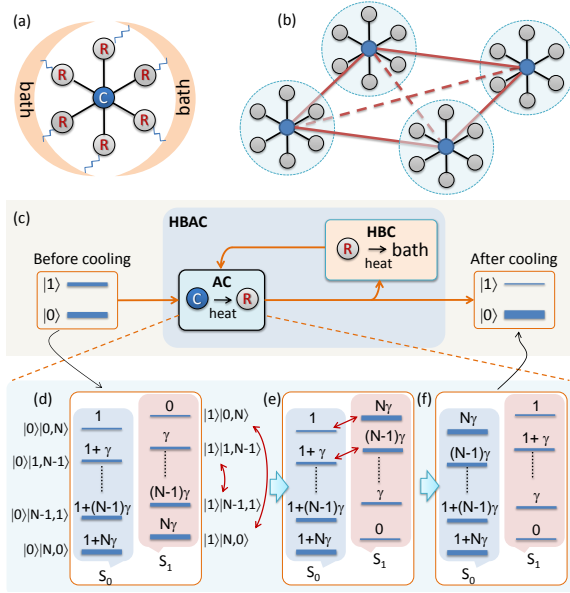


FIG. 1. (a) Star-topology with a central computation qubit and a set of reset qubits surrounded by a bath, (b) a four-star quantum register, (c) HBAC procedure. The different steps of AC are illustrated in (d-f). In (d) the various levels are labeled as $|\alpha\rangle|N-j, j\rangle$, where $\alpha = \{0, 1\}$ corresponds to the two states of the computation qubit and $j \in \{0, \dots, N\}$ denotes the number of reset qubits in state $|1\rangle$.

The Hamiltonian of such a star-system in a doubly rotating frame is

$$\mathcal{H} = -\frac{\hbar\omega_C}{2}\sigma_z^C - \frac{\hbar\omega_R}{2}\sum_{j=1}^N\sigma_{jz}^R + \frac{\hbar\pi J_{RC}}{2}\sum_{j=1}^N\sigma_z^C\sigma_{jz}^R, \quad (1)$$

where σ_z represents the Pauli operator and ω_C , ω_R are tunable resonance off-sets which can be set to zero without loss of generality.

Once cooled, the computation qubit should ideally remain in the low-entropy state for a long time. To that end, it needs to be sufficiently isolated from the bath and thereby have a long memory in terms of its spin lattice relaxation time T_1^C . On the other hand, the reset qubits need to strongly interact with the bath, and should ideally have a short T_1^R so that many cycles of HBAC can be performed. This requirement is very well satisfied by the star-topology systems wherein the outer reset qubits seem to shield the central computation qubit from the environmental influences.

At high-temperature ($kT \gg \hbar\omega_C$) limits, the thermal-equilibrium density matrix ρ_{eq}^C of the computation qubit can be approximated as a convex sum of the maximally mixed state ($\mathbb{1}/2$) and a *deviation* (ρ_{Δ}^C), i.e.,

$$\rho_{\text{eq}}^C = \frac{1}{2}\exp\left(\frac{\hbar\omega_C\sigma_z^C}{2kT}\right) \approx (1-\epsilon)\frac{\mathbb{1}}{2} + \epsilon|0_C\rangle\langle 0_C| \quad (2)$$

in the eigenbasis $\{|0_C\rangle, |1_C\rangle\}$ of the Zeeman Hamiltonian. Here the dimensionless quantity $\epsilon = \hbar\omega_C/(2kT)$ is a mea-

sure of the purity of the thermal state.

Spin temperature T^C for an arbitrary single-qubit state ρ^C , with diagonal elements ρ_{00}^C and ρ_{11}^C and null off-diagonal elements in the Zeeman basis, is quantified by the Boltzmann distribution,

$$\frac{\rho_{11}^C}{\rho_{00}^C} = \exp\left[-\frac{\hbar\omega_0^C}{kT^C}\right]. \quad (3)$$

While $T^C = T$ at thermal equilibrium, the objective is to *cool* the computation qubit such that $T^C \ll T$ by redistributing ρ_{00}^C and ρ_{11}^C . As shown in Fig. 1 (c), we can achieve cooling by transferring the magnetization iteratively from reset qubits to the computation qubit. Each iteration involves two stages - (i) algorithmic cooling (AC), wherein entropy is transferred from the computation qubit to the reset qubit, and (ii) heat-bath cooling (HBC), wherein the reset qubits give away the extra entropy gained to the bath. Together these stages form heat-bath algorithmic cooling (HBAC).

B. HBAC in Star-topology Quantum Registers

First we explain AC in star-registers which involves a two-step procedure. The 2^{N+1} energy-levels of the $N+1$ star-register, can be grouped into two subspaces S_0 and S_1 corresponding to $|0\rangle$ and $|1\rangle$ states of the computation qubit (see Fig. 1 (d)), such that the deviation matrix

$$\rho_{\Delta} = |0_C\rangle\langle 0_C| \otimes S_0 + |1_C\rangle\langle 1_C| \otimes S_1. \quad (4)$$

In each subspace S_{α} , the star-symmetry imposes degeneracy in all the levels except in the ground and the most-excited levels. Degeneracy of the level $|\alpha\rangle|N-j, j\rangle$ in Fig. 1 (d) is ${}^N C_j = N!/j!(N-j)!$.

The two subspaces S_0 and S_1 are identical, except that S_1 has a higher energy and therefore a lower population. The first step in AC involves the population inversion of S_1 (see Fig. 1 (d) and (e)). It can be realized experimentally by applying a transition-selective π pulse on the common $+J/2$ transition of the reset qubits. The second-step involves inverting top m transitions of the computation qubit (see Fig. 1 (e) and (f)). One might naively choose $m = \lfloor N/2 \rfloor$, the largest integer less than or equal to $N/2$. However, numerical calculations suggest that there exists an optimum m for a given star-system (Appendix A). Of course, it also depends on the total number as well as the fidelity of HBAC iterations. These two operations of AC drive a large population from S_1 to S_0 and in effect transfer the entropy to reset qubits. The next step is HBC which simply involves a delay τ_{HB} that is just long enough for the reset qubits to release the excess entropy to the heat bath. An excess delay will undesirably allow the computation-qubit to heat-up again (Appendix A 4). AC and HBC together form one iteration of HBAC. After sufficiently many HBAC iterations, the reset qubits are traced out, and the cooled computation qubit can be used for further processing.

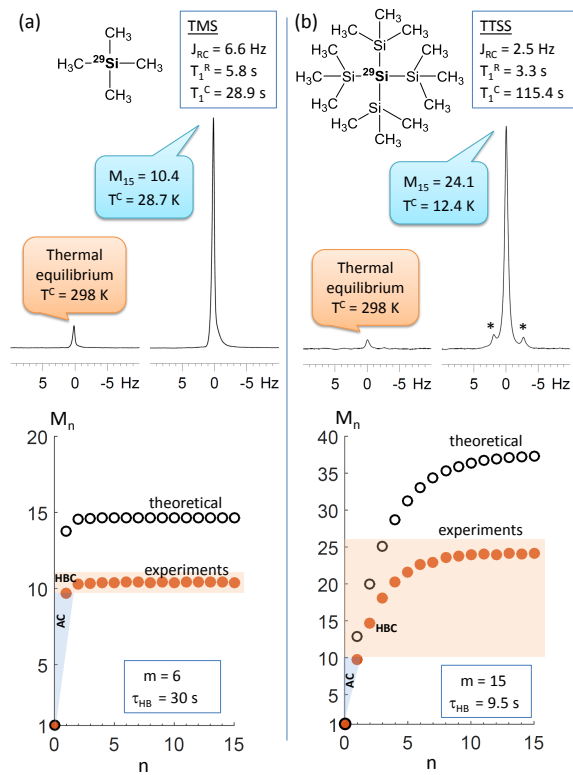


FIG. 2. HBAC of (a) TMS and (b) TTSS. Shown in each case are - molecular structure, ^1H -decoupled ^{29}Si spectra before and after HBAC, and magnetization versus HBAC iteration number (n). Here the theoretical data-points are calculated with ideal HBAC controls. In the right spectrum, the sidebands (indicated by stars) are due to ^{29}Si - ^{13}C J-coupling.

C. Estimation of Cooling

We now describe numerical estimation of HBAC efficiency in a star-system. The dynamics of relative populations and hence that of the longitudinal magnetization of a pair of levels with a spin-lattice relaxation time T_1 follows Bloch's equation [27]. However, for a star-system with $(N + 1)$ -qubits, tracking all the populations (2^{N+1}) appears to be a daunting task. Nevertheless, by exploiting the symmetry of the star-system as well as the time-scale separation between the memories of \mathbf{C} and \mathbf{R} qubits (i.e., $T_1^{\mathbf{C}} \gg T_1^{\mathbf{R}}$), we can analyze the population dynamics and calculate the relative magnetization M_n and the corresponding spin temperature $T_n^{\mathbf{C}}$ after n^{th} iteration (Appendix A). In NMR, $kT_n^{\mathbf{C}} \gg \hbar\omega_0^{\mathbf{C}}$, and therefore

$$T^{\mathbf{C}}(n) \simeq T/M_n, \quad (5)$$

where we have set $M_0 = 1$ as the thermal equilibrium magnetization at the sample temperature T .

III. EXPERIMENTS

A. HBAC in 13-star and 37-star systems

We performed HBAC in (i) 13-star system: tetramethylsilane (TMS) (Fig. 2 (a)) as well as (ii) 37-star system: tetrakis(trimethylsilyl)silane (TTSS) (Fig. 2 (b)), each dissolved in CDCl_3 . In both cases, all the ^1H spins act as reset qubits and the central naturally-abundant ^{29}Si spin acts as the computation qubit. The coupling constants (J_{RC}), T_1 values, the number of swapped energy levels (m), and heat-bath durations (τ_{HB}) used in the experiments are displayed in Fig. 2. All the experiments were carried out in a 400 MHz Bruker NMR spectrometer at an ambient temperature of 298 K.

The subspace inversion in the first part of AC (see Fig. 1 (d)) was achieved by a transition-selective Gaussian-shaped π pulse of duration 750 ms which was on-resonant on the ^1H transition corresponding to S_1 subspace. The second part of AC involving inter-subspace swapping of top m energy-levels (see Fig. 1 (e)) was achieved by an amplitude and phase modulated RF pulse which inverts only the transitions with positive frequencies [Appendix B]. The heat-bath delay τ_{HB} was set to 30 s and 9.5 s for TMS and TTSS respectively. Finally, we measured ^{29}Si magnetization (M_n) from the ^1H decoupled ^{29}Si spectra recorded versus the HBAC iteration-number (n). The experimental results are compared with numerical predictions in Fig. 2. Representative ^{29}Si spectra comparing before and after HBAC are also shown in Fig. 2. In the case of TMS, the magnetization after 15 HBAC iterations was enhanced by a factor of 10.4, which corresponds to a spin temperature of 28.7 K. In the case of TTSS, the enhancement factor after 15 HBAC iterations was 24.1, which corresponds to a spin temperature of 12.4 K.

The numerically predicted upper-bounds for the magnetizations under perfect HBAC iterations are also shown in Fig. 2. Comparison of the theoretical limits with the experimental results suggests a scope for further enhancement of cooling. The lower values of experimentally obtained cooling are mainly due to finite fidelity of GRAPE pulses, RF inhomogeneities, decoherence, and nonlinearities in the spectrometer hardware. Quantitative details on the imperfections are described in appendix (Appendix A 2).

B. Achieving large combination-coherences

As an immediate application of the strong polarization obtained by HBAC, we prepare and filter-out large combination coherences [28], which are essential in realizing a scalable quantum processor. The quantum circuit for studying such coherences is shown in Fig. 3 (a). For a star-system with even- N , the q -quantum combination coherence appears as a single transition with a frequency $(q - 1)J_{\text{RC}}/2$ from the central transition. The experimental spectra corresponding to odd-quantum co-

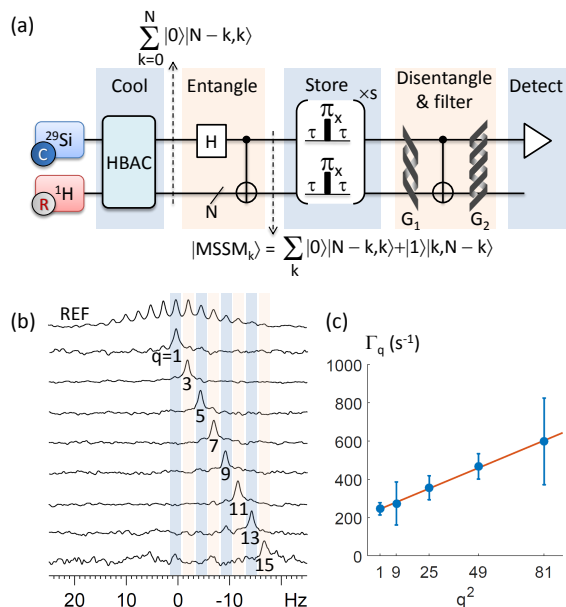


FIG. 3. (a) Quantum circuit for preparing combination coherences. Here due to the star-symmetry, each CNOT gate acts simultaneously on all the reset qubits. A pair of pulsed-field-gradients G_1 and G_2 select a coherence of order- q which is converted into an observable single-quantum coherence by the second CNOT [25]. (b) ^{29}Si reference spectrum of TTSS and characteristic spectra corresponding to various coherences of odd orders q . (c) The decay rates (Γ_q) versus q^2 measured in TTSS.

herences with orders up to 15 are displayed in Fig. 3 (b).

Further, as indicated by the circuit in Fig. 3 (a), we benchmark the life-time of various coherences (with orders from $q = 1$ to 9) under the CP storage [29] with an inter-pulse delay $2\tau = 500 \mu\text{s}$. Tang and Pines [30] had earlier predicted that in the case of completely correlated noise, the adiabatic term of the relaxation rate Γ_q originated from the energy-conserving processes is proportional to the square of the coherence order, i.e., $\Gamma_q \propto q^2$. Fig. 3 (c) displays a good linear fit of Γ_q versus q^2 for TTSS. It is interesting to note that the noise in TTSS is hence predominantly correlated. It may also be noted that benchmarking in a 12-qubit system was earlier reported by Negrevergne et al [31].

C. A pair of computation qubits

We now describe HBAC of a pair of computation qubits using two naturally abundant ^{29}Si spins of pentamethyldisilane (PDS) dissolved in CDCl_3 (see Fig. 4). The RF off-set was chosen such that the resonance frequencies of the two ^{29}Si spins were $\pm 806 \text{ Hz}$, and their T_1 values are 47.2 s and 39.5 s respectively. T_1 values of ^1H spins are about 8.5 s. The coupling between the methyl protons and the closest ^{29}Si was 6.5 Hz while that

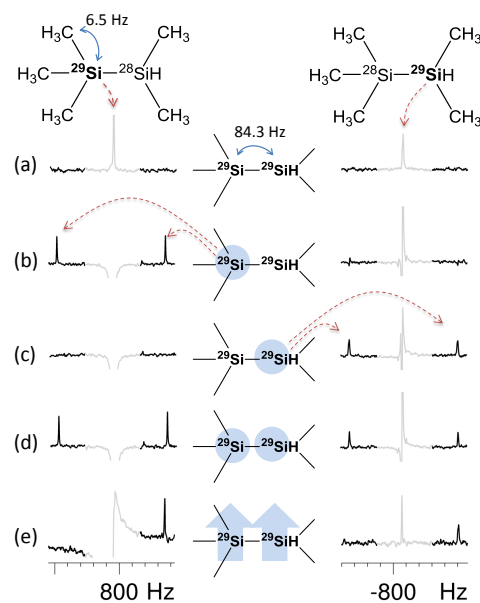


FIG. 4. HBAC of a pair of computation qubits. (a) The reference spectra of ^{29}Si corresponding to the thermal equilibrium magnetization. Spectra obtained after (b) cooling the left qubit, (c) transferring the polarization from left qubit to right qubit, (d) cooling the left qubit again, and (e) finally preparing the two ^{29}Si qubits in the $|00\rangle$ pseudopure state.

between the two ^{29}Si spins was 84.3 Hz.

The spectra corresponding to thermal equilibrium magnetization are shown in Fig. 4 (a). The two central peaks (de-emphasized) at $\pm 806 \text{ Hz}$ correspond to those molecules wherein only one of the silicons is ^{29}Si , while the other being NMR-inactive ^{28}Si (spin-0 nucleus). Here, no signal from a pair of interacting qubits (^{29}Si - ^{29}Si) can be observed. Fig. 4 (b) displays the spectra obtained after algorithmic cooling (AC) of the left qubit, while the right qubit remains unobservable. The pair of spectral lines in the left qubit is due to splitting caused by ^{29}Si - ^{29}Si J-coupling. We then transferred the polarization from left qubit to right qubit using a SWAP gate. As evident in the spectra displayed in Fig. 4 (c), the pair of lines in the left disappear, while the corresponding pair in the right appear. After a heat-bath delay of 20 s, we carryout a second algorithmic cooling of the left qubit, so that both the qubits are now polarized as indicated by Fig. 4 (d). Finally we prepare $|00\rangle$ pseudopure state of the two cooled qubits using spatial averaging technique [32]. The pair of qubits are now ready for implementing quantum gates or any other algorithms.

IV. SUMMARY AND DISCUSSIONS

We proposed an arrangement of star-topology quantum registers that allows cryorefrigeration of spin-qubits by drastically reducing the spin temperature. Here each of the computation qubits is surrounded by a symmet-

ric set of reset-qubits. We described the heat-bath algorithmic cooling of computation qubits by iterating a two-step procedure of transferring entropy from the computation qubits to the reset qubits and subsequently to a heat bath. Using NMR techniques, we experimentally demonstrated the heat-bath algorithmic cooling in two different star-systems of 13 and 37 spins respectively. We obtained strong polarization enhancements up to a factor of over 24 which reduces the spin-temperature from room-temperature down to 12 K. Using a ^{29}Si qubit with a natural abundance of mere 4.6% as the computation qubit, we were able to prepare combination quantum coherences of orders up to 15. By measuring the life-times of these coherences we studied the noise characteristics in the 37-spin system. Further, on another system having a naturally abundant pair of ^{29}Si , we demonstrated a sequential heat-bath algorithmic cooling and subsequently prepared a pseudopure state.

Star-topology registers promise interesting applications in a variety of quantum devices wherein robust cooling of computation qubits is necessary. In an addressable array of star-registers, it is possible to achieve further cooling by incorporating the above method with other entropy compression schemes. The present work may also have ramifications in the spectroscopy of low natural-abundance nuclear isotopes such as ^{29}Si demonstrated in this work. In principle, it is possible to combine the method described here with hyperpolarization techniques to achieve higher cooling. Further, by using a stronger magnetic field and a sophisticated detection hardware such as a cryo-probe one can prepare and detect higher coherence orders.

ACKNOWLEDGMENTS

Authors acknowledge V. S. Anjusha and Sudheer Kumar for discussions. This work was partly supported by DST/SJF/PSA-03/2012-13 and CSIR 03(1345)/16/EMR-II. VRP and GB acknowledge support from DST-INSPIRE fellowship.

Appendix A: Numerical estimation of HBAC in star-topology registers

1. Population SWAPs

The traditional way to treat the relaxation in a multi-level system is via Solomon equations [33]. However, here we provide a simpler analysis by exploiting the symmetry of the star-system as well as the fact that reset qubits have much shorter memory than the computation qubit, i.e., $T_1^R \ll T_1^C$. This condition is very well satisfied by the experimental spin-systems described in the text. The time-scale separation implies the following: on disturbing the thermal equilibrium state, the intra-subspace transitions quickly re-establish Boltzmann distribution within

each subspace, while the inter-subspace transitions take place at a much slower rate. Although the thermal equilibrium is established eventually, we are interested in the intermediate time scales at which the inter-subspace population difference is maximized, and hence higher magnetization is achieved.

Consider a subspace S_α of Fig. 1 (d) of the main text. Consistent with the high-temperature Boltzmann distribution, the equilibrium populations of j th eigenstates in S_0 and S_1 are set to (up to a scaling factor)

$$p_j^0 = b_j \quad \text{and} \quad p_j^1 = b_j - 1 \quad (\text{A1})$$

respectively, where $b_j = b + 1 + \gamma(N - j)$ with b being the uniform background population. Thus, up to a uniform background and a scaling, the population difference between a pair of levels connected by reset-qubit transition (intra-subspace) is γ , while that connected by a computation qubit transition (inter-subspace) is normalized to be 1. The populations of ${}^N C_j$ -fold degenerate levels $|0\rangle|N - j, j\rangle$ and $|1\rangle|N - j, j\rangle$ are

$$\begin{aligned} B_j^0 &= {}^N C_j b_j \quad \text{and} \\ B_j^1 &= {}^N C_j (b_j - 1), \end{aligned} \quad (\text{A2})$$

and $B^0 = \sum_j B_j^0$, $B^1 = \sum_j B_j^1$ are the total populations of the two subspaces respectively. The thermal equilibrium magnetization M_0 of the computation qubit is proportional to the inter-subspace population difference, i.e.,

$$M_0 = m_c(B^0 - B^1) = m_c \sum_j {}^N C_j = m_c 2^N, \quad (\text{A3})$$

where m_c is a proportionality constant. Without loss of generality, we can set $M_0 = 1$.

The first step of the algorithmic cooling involves the population-inversion of S_1 , while the second step involves swapping the top $m < \lfloor N/2 \rfloor$ transitions (here $\lfloor x \rfloor$ indicates the greatest integer less than or equal to x) of the computation qubit. Effectively, it results in the population swapping of top-half of S_0 with bottom-half of S_1 , i.e.,

$$\begin{aligned} p_j^0 &\xrightarrow{\eta_j} (1 - \eta_j)p_j^0 + \eta_j p_{N-j}^1, \quad \text{and} \\ p_{N-j}^1 &\xrightarrow{\eta_j} (1 - \eta_j)p_{N-j}^1 + \eta_j p_j^0, \end{aligned} \quad (\text{A4})$$

where η_j denotes swapping factor. Although ideally

$$\eta_j = \begin{cases} 1 & \text{for } j > N - m \\ 0 & \text{otherwise,} \end{cases}$$

imperfections of practical SWAP gates lead to lower degree of algorithmic cooling. The populations of various levels of either subspaces (at time $t=0$ indicated by the parenthesis) are now

$$\begin{aligned} p_j^0(0) &= (1 - \eta_j)b_j + \eta_j(b_{N-j} - 1), \quad \text{and} \\ p_{N-j}^1(0) &= (1 - \eta_j)(b_{N-j} - 1) + \eta_j b_j. \end{aligned} \quad (\text{A5})$$

Denoting the initial subspace populations by

$$\begin{aligned} P^0(0) &= \sum_j^N C_j p_j^0(0), \text{ and} \\ P^1(0) &= \sum_j^N C_j p_j^1(0), \end{aligned} \quad (\text{A6})$$

the relative magnetization of computation qubit for the first cooling iteration

$$M_1 = \frac{P^0(0) - P^1(0)}{B^0 - B^1}. \quad (\text{A7})$$

If now a heat bath delay is introduced, the inter-subsystem transitions slowly drive the computation qubit towards thermal equilibrium via Bloch equation, i.e.,

$$M(\tau) = 1 + (M_1 - 1)e^{-\tau/T_1^c}. \quad (\text{A8})$$

For the second iteration, before we can calculate the effect of SWAP operation (Eq. A4), we need to know the populations of various levels in each subspace. This is described in the following.

2. Intra-subspace relaxation

For the moment, we ignore the inter-subspace relaxation which occurs at a much slower rate. For simplicity, let us consider only S_0 subspace, but similar calculations hold for S_1 as well. Consider a pair of energy levels $(j, j+1)$ connected by the reset qubit transition with energy $\hbar\omega_R$ and prepared with initial populations $p_{j+1}^0(0)$ and $p_j^0(0)$. The initial magnetization is proportional to the population difference $\Delta p_{j,j+1}^0(0) = \{p_j^0(0) - p_{j+1}^0(0)\}$, i.e.,

$$M_R^{j,j+1}(0) = m_R \Delta p_{j,j+1}, \quad (\text{A9})$$

and it gradually evolves towards the equilibrium magnetization $m_R\gamma$ via Bloch equation such that the instanta-

neous magnetization

$$M_R^{j,j+1}(\tau) = m_R\gamma + [M_R^{j,j+1}(0) - m_R\gamma]e^{-\tau/T_1^R}. \quad (\text{A10})$$

Thus, in terms of populations we obtain,

$$p_j^0(\tau) - p_{j+1}^0(\tau) = \gamma + \{\Delta p_{i,i+1}^0(0) - \gamma\}e^{-\tau/T_1^R}, \quad (\text{A11})$$

where all terms in the right hand side are already known. Thus, in the multi-level system with $(N+1)$ -unknowns $p_j(\tau)$, we obtain a set of N coupled linear equations. Solving these equations together with the overall population conserving equation

$$\sum_j^N C_j p_j^0(\tau) = \sum_j^N C_j p_j^0(0), \quad (\text{A12})$$

we can determine all the temporal populations in S_0 . Similarly, we can determine the populations in S_1 .

3. Inter-subspace relaxation

We assume that all the transitions of the computation qubit have the same relaxation time constant T_1^c . In that case, using Eq. A8

$$p_j^0(\tau) - p_j^1(\tau) = 1 + \{p_j^0(0) - p_j^1(0) - 1\}e^{-\tau/T_1^c} \quad (\text{A13})$$

Using above equation along with $p_j^0(\tau) + p_j^1(\tau) = p_j^0(0) + p_j^1(0)$, we can determine $p_j^0(\tau)$ and $p_j^1(\tau)$.

We can now calculate the effect of SWAP (Eq. A4) and thereby estimate the relative magnetization M_2 for the 2nd iteration of HBAC. In addition, by interpolating the experimentally obtained magnetizations M_n we can also estimate the swapping factors η_j . Fig. 5 shows the swapping factors for both TMS and TTSS.

4. Variation of M_{15} with N , m and τ_{HB}

In the following we describe some interesting scenarios as predicted by the above model of HBAC in star-topology systems. First of all, for a given set of HBAC parameters $(T_1^R, T_1^c, \tau_{HB})$ we find a zig-zag pattern for magnetization (M_n) as a function of size of the star (N). Fig. 6 displays M_n versus N curves for a range of γ values. Interestingly, HBAC efficiency is higher for odd values of N . Of course, these profiles depend on the number of high-energy transitions (of computation qubit) which are being swapped. For a given system, it might be possible to optimize this number for various iterations to achieve the best cooling rate.

Secondly, we also show the dependence of magnetization on the heat-bath delay τ_{HB} . Fig. 7 (b) illustrates this dependence for a particular set of parameters. As expected, there is an optimum delay at which maximum cooling can be achieved.

Another interesting optimization parameter is m , the

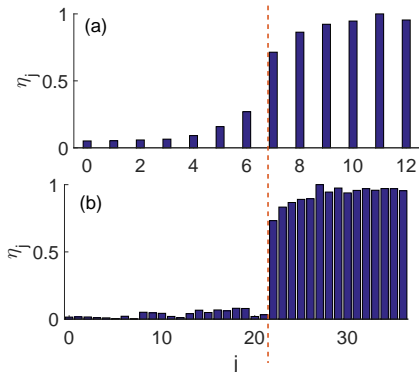


FIG. 5. Estimated swapping factors η_j versus the transition number j of the computation qubit in (a) TMS and (b) TTSS as indicated.

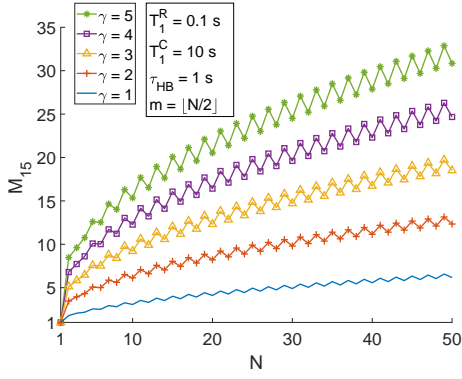


FIG. 6. Simulated magnetizations after 15 iterations of HBAC versus star-size (N) for a set of relative gyromagnetic ratios (γ). The HBAC parameters are shown in the inset.

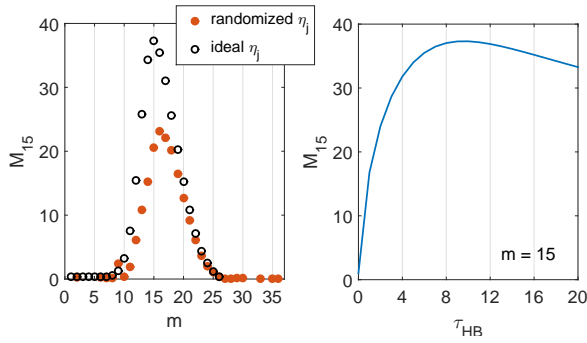


FIG. 7. (a) Simulated magnetization of TTSS versus the number of top-levels swapped (m) during HBAC iterations. In the case of randomized η_j values, $\eta_j = 0$ and $\eta_j = 1$ are replaced with distributions $[0, 0.2]$ and $[0.8, 1]$ respectively. (b) Magnetization versus the heat-bath delay.

number of transitions of the computation-qubit to be inverted during HBAC iterations. Fig. 7 (a) displays the numerical simulation of M_{15} versus m . It appears that for a system with finite memories (T_1^R , T_1^C), generally $m < \lfloor N/2 \rfloor$. In fact, one can also vary the m value during the HBAC iterations.

Appendix B: Specially designed RF controls

For AC, we need to invert only the top-half of the populations, i.e., only the positive transitions of the computation qubit. In order to design such a pulse, we assumed a set of about 50 two-level systems whose resonance offset are uniformly spread over a range from -50 Hz to 50 Hz. An RF pulse for the selective inversion of half the transitions was then numerically obtained by modifying the GRAPE algorithm [35]. The inversion profile of the single-step GRAPE pulse and its experimental

performance-analysis are shown in Fig. 8.

Although one can use standard shaped-pulses such as I-BURP to achieve band-selective inversion, we observed

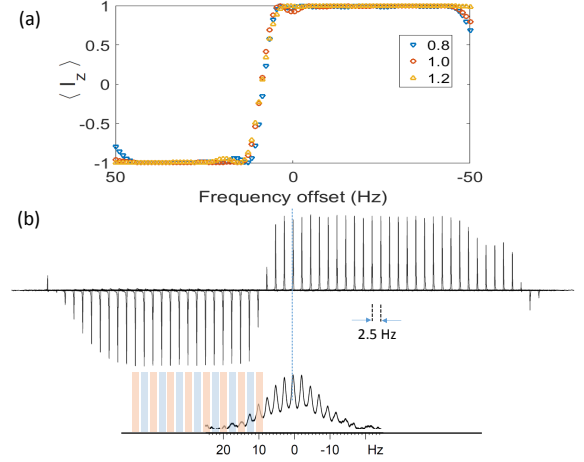


FIG. 8. (a) The inversion profile of the single-step GRAPE pulse. To illustrate its robustness w.r.t. RF inhomogeneity, three inversion profiles with 0.8, 1.0, and 1.2 times the nominal RF amplitudes are displayed. (b) Performance of the single-step GRAPE pulse experimentally observed by shifting a single-resonance peak. The reference spectrum of TTSS is shown at the bottom. First 15 lines of TTSS are inverted since $m = 15$ (see main text).

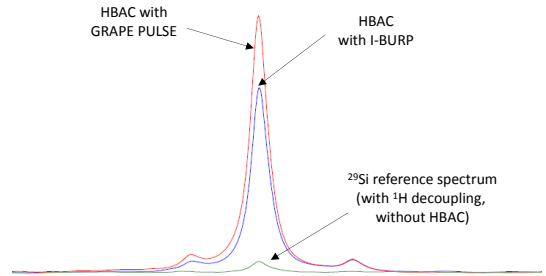


FIG. 9. Comparing the HBAC performance of the single-step GRAPE pulse with IBURP-1 [34].

better performance with the robust GRAPE pulse generated by us (see Fig. 9).

In the case of HBAC of a pair of qubits, each ^{29}Si transition is split by ^{29}Si - ^{29}Si coupling followed by ^{29}Si - ^1H coupling. Therefore, to cool one of the ^{29}Si qubits (say left one as indicated in Fig. 4 in the main text) we need to invert two sets - each of m transitions - corresponding only to top m energy levels of ^1H . This requires a pair of inversion and no-inversion zones. Using the pulse-shaping methods described above we designed such a double-step GRAPE pulse (see Fig. 10).

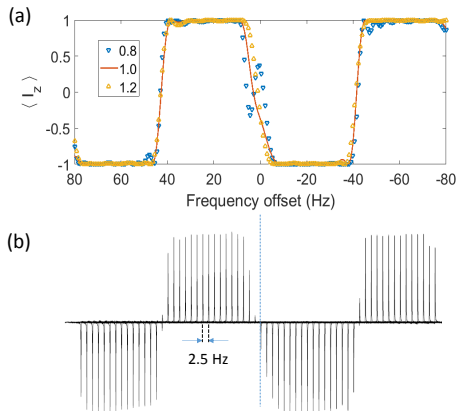


FIG. 10. (a) The inversion profile of the double-step GRAPE pulse. To illustrate its robustness w.r.t. RF inhomogeneity, three inversion profiles with 0.8, 1.0, and 1.2 times the nominal RF amplitudes are displayed. (b) Performance of the double-step GRAPE pulse experimentally observed by shifting a single-resonance peak.

-
- [1] D. P. DiVincenzo, “The physical implementation of quantum computation,” *Fortschritte der Physik*, vol. 48, p. 771, 2000.
- [2] J. Cirac, A. Ekert, and C. Macchiavello, “Optimal purification of single qubits,” *Physical review letters*, vol. 82, no. 21, p. 4344, 1999.
- [3] D. K. Park, N. A. Rodriguez-Briones, G. Feng, R. Rahimi, J. Baugh, and R. Laflamme, “Heat bath algorithmic cooling with spins: review and prospects,” pp. 227–255, 2016.
- [4] T. Chakraborty, J. Zhang, and D. Suter, “Polarizing the electronic and nuclear spin of the nv-center in diamond in arbitrary magnetic fields: analysis of the optical pumping process,” *New Journal of Physics*, 2017.
- [5] M. S. Anwar, J. A. Jones, D. Blazina, S. B. Duckett, and H. A. Carteret, “Implementation of nmr quantum computation with parahydrogen-derived high-purity quantum states,” *Phys. Rev. A*, vol. 70, p. 032324, Sep 2004.
- [6] G. A. Morris and R. Freeman, “Enhancement of nuclear magnetic resonance signals by polarization transfer,” *Journal of the American Chemical Society*, vol. 101, no. 3, pp. 760–762, 1979.
- [7] O. W. Sørensen, “Polarization transfer experiments in high-resolution nmr spectroscopy,” *Progress in Nuclear Magnetic Resonance Spectroscopy*, vol. 21, no. 6, pp. 503–569, 1989.
- [8] L. J. Schulman and U. V. Vazirani, “Molecular scale heat engines and scalable quantum computation,” in *Proceedings of the thirty-first annual ACM symposium on Theory of computing*, pp. 322–329, ACM, 1999.
- [9] P. O. Boykin, T. Mor, V. Roychowdhury, F. Vatan, and R. Vrijen, “Algorithmic cooling and scalable nmr quantum computers,” *Proceedings of the National Academy of Sciences*, vol. 99, no. 6, pp. 3388–3393, 2002.
- [10] J. M. Fernandez, S. Lloyd, T. More, and V. Roychowdhury, “Algorithmic cooling of spins: A practicable method for increasing polarization,” *International Journal of Quantum Information*, vol. 02, no. 04, pp. 461–477, 2004.
- [11] L. J. Schulman, T. Mor, and Y. Weinstein, “Physical limits of heat-bath algorithmic cooling,” *Phys. Rev. Lett.*, vol. 94, p. 120501, Apr 2005.
- [12] Y. Elias, J. M. Fernandez, T. Mor, and Y. Weinstein, “Optimal algorithmic cooling of spins,” *Israel Journal of Chemistry*, vol. 46, no. 4, pp. 371–391, 2006.
- [13] L. J. Schulman, T. Mor, and Y. Weinstein, “Physical limits of heatbath algorithmic cooling,” *SIAM Journal on Computing*, vol. 36, no. 6, pp. 1729–1747, 2007.
- [14] Y. Elias, T. Mor, and Y. Weinstein, “Semi-optimal practicable algorithmic cooling,” *Phys. Rev. A*, vol. 83, p. 042340, Apr 2011.
- [15] D. E. Chang, L. M. Vandersypen, and M. Steffen, “Nmr implementation of a building block for scalable quantum computation,” *Chemical physics letters*, vol. 338, no. 4, pp. 337–344, 2001.
- [16] J. M. Fernandez, T. Mor, and Y. Weinstein, “Paramagnetic materials and practical algorithmic cooling for nmr quantum computing,” *International Journal of Quantum Information*, vol. 03, no. 01, pp. 281–285, 2005.
- [17] J. Baugh, O. Moussa, C. A. Ryan, A. Nayak, and R. Laflamme, “Experimental implementation of heat-bath algorithmic cooling using solid-state nuclear magnetic resonance,” *Nature*, vol. 438, no. 7067, pp. 470–473, 2005.
- [18] Y. Elias, H. Gilboa, T. Mor, and Y. Weinstein, “Heat-bath cooling of spins in two amino acids,” *Chemical Physics Letters*, vol. 517, no. 46, pp. 126 – 131, 2011.
- [19] D. K. Park, G. Feng, R. Rahimi, S. Labruyère, T. Shibata, S. Nakazawa, K. Sato, T. Takui, R. Laflamme, and J. Baugh, “Hyperfine spin qubits in irradiated malonic

- acid: heat-bath algorithmic cooling,” *Quantum Information Processing*, vol. 14, no. 7, pp. 2435–2461, 2015.
- [20] C. Ryan, O. Moussa, J. Baugh, and R. Laflamme, “Spin based heat engine: demonstration of multiple rounds of algorithmic cooling,” *Physical review letters*, vol. 100, no. 14, p. 140501, 2008.
- [21] Y. Atia, Y. Elias, T. Mor, and Y. Weinstein, “Algorithmic cooling in liquid-state nuclear magnetic resonance,” *Physical Review A*, vol. 93, no. 1, p. 012325, 2016.
- [22] S. Raeisi and M. Mosca, “Asymptotic bound for heat-bath algorithmic cooling,” *Phys. Rev. Lett.*, vol. 114, p. 100404, Mar 2015.
- [23] N. A. Rodríguez-Briones and R. Laflamme, “Achievable polarization for heat-bath algorithmic cooling,” *Phys. Rev. Lett.*, vol. 116, p. 170501, Apr 2016.
- [24] J. A. Jones, S. D. Karlen, J. Fitzsimons, A. Ardavan, S. C. Benjamin, G. A. D. Briggs, and J. J. L. Morton, “Magnetic field sensing beyond the standard quantum limit using 10-spin noon states,” *Science*, vol. 324, no. 5931, pp. 1166–1168, 2009.
- [25] A. Shukla, M. Sharma, and T. Mahesh, “Noon states in star-topology spin-systems: Applications in diffusion studies and rf inhomogeneity mapping,” *Chemical Physics Letters*, vol. 592, pp. 227–231, 2014.
- [26] D. Khurana, G. Unnikrishnan, and T. Mahesh, “Spectral investigation of the noise influencing multiqubit states,” *Physical Review A*, vol. 94, no. 6, p. 062334, 2016.
- [27] F. Bloch, “Nuclear induction,” *Physical review*, vol. 70, no. 7-8, p. 460, 1946.
- [28] M. H. Levitt, *Spin dynamics: basics of nuclear magnetic resonance*. John Wiley & Sons, 2001.
- [29] H. Y. Carr and E. M. Purcell, “Effects of diffusion on free precession in nuclear magnetic resonance experiments,” *Physical review*, vol. 94, no. 3, p. 630, 1954.
- [30] J. Tang and A. Pines, “Multiple quantum nmr and relaxation of an oriented ch₃ group,” *The Journal of Chemical Physics*, vol. 72, no. 5, pp. 3290–3297, 1980.
- [31] C. Negrevergne, T. Mahesh, C. Ryan, M. Ditty, F. Cyr-Racine, W. Power, N. Boulant, T. Havel, D. Cory, and R. Laflamme, “Benchmarking quantum control methods on a 12-qubit system,” *Physical Review Letters*, vol. 96, no. 17, p. 170501, 2006.
- [32] D. G. Cory, A. F. Fahmy, and T. F. Havel, “Ensemble quantum computing by nmr spectroscopy,” *Proceedings of the National Academy of Sciences*, vol. 94, no. 5, pp. 1634–1639, 1997.
- [33] I. Solomon, “Relaxation processes in a system of two spins,” *Physical Review*, vol. 99, no. 2, p. 559, 1955.
- [34] H. Geen and R. Freeman, “Band-selective radiofrequency pulses,” *Journal of Magnetic Resonance (1969)*, vol. 93, no. 1, pp. 93–141, 1991.
- [35] N. Khaneja, T. Reiss, C. Kehlet, T. Schulte-Herbrüggen, and S. J. Glaser, “Optimal control of coupled spin dynamics: design of nmr pulse sequences by gradient ascent algorithms,” *Journal of magnetic resonance*, vol. 172, no. 2, pp. 296–305, 2005.